Weak decay of halo nuclei

Wael Elkamhawy [1,*] Hans-Werner Hammer [1,2,†] and Lucas Platter [3,4,1,2,‡]
[1]*Institut für Kernphysik, Technische Universität Darmstadt, 64289 Darmstadt, Germany*
[2]*ExtreMe Matter Institute EMMI and Helmholtz Forschungsakademie Hessen für FAIR (HFHF), GSI Helmholtzzentrum für Schwerionenforschung GmbH, 64291 Darmstadt, Germany*
[3]*Department of Physics and Astronomy, University of Tennessee, Knoxville, Tennessee 37996, USA*
[4]*Physics Division, Oak Ridge National Laboratory, Oak Ridge, Tennessee 37831, USA*

(Received 19 December 2022; revised 1 May 2023; accepted 14 June 2023; published 7 July 2023)

We investigate the weak decay of one-neutron halo nuclei into the proton-core continuum, i.e., β-delayed proton emission from the halo nucleus using a cluster effective field theory for halo nuclei. On the one hand, we calculate the direct decay into the continuum. On the other hand, we consider the case of resonant final state interactions between the proton and the core. We present our formalism and discuss the application to the decay of ^{11}Be in detail. Moreover, we compare to recent experimental results for the branching ratio and resonance parameters. As another example, we consider the case of ^{19}C and predict the branching ratio for β-delayed proton emission.

DOI: 10.1103/PhysRevC.108.015501

"

I. INTRODUCTION

Halo nuclei are exotic nuclei showing a pronounced cluster structure. They consist of a tightly bound core nucleus and a few weakly bound valence nucleons. Halo nuclei thus exhibit a reduction in the number of degrees of freedom since the many-body nucleus can be described as an effective few-body system and thereby a different and smaller set of parameters. This transition to different degrees of freedom is signaled by a separation of scales that is also apparent in observables. In halo nuclei, the scales $R_{\rm core}$ and $R_{\rm halo}$ that denote the length scales of the core and halo, respectively, are clearly separated such that the ratio $R_{\rm core}/R_{\rm halo} \ll 1$ can be used as an expansion parameter. One can then construct an effective field theory (EFT) to calculate halo observables in a systematic expansion in $R_{\rm core}/R_{\rm halo}$ using only the new *effective* degrees of freedom [1,2]. This EFT for halo nuclei is known as halo EFT and has been applied successfully to many halo nuclei (see Refs. [3–5] for recent reviews). This separation of scales also leads to other universal features, such as the dependence of matrix elements on only a couple of few-body parameters. For example, the one-neutron separation energy of an S-wave one-neutron halo is directly related to the core-neutron scattering length. Similar relations exist for other static properties, such as the matter or charge radii, and reaction rates such as neutron capture.

Another less obvious candidate for a halo physics-dominated observable is the weak decay rate: One might expect that the decay rate of a one-neutron halo nucleus is determined by the weakly bound neutron, provided the core half-life is significantly larger than the neutron half-life. However, such decays can be dominated by transitions into deeply bound states of the daughter nucleus since the total decay rate depends on the available phase space, which is larger when more energy is released. Nonetheless, one can still identify the channel in which a proton is emitted into the continuum as originating from the decay of the halo neutron. For ^{11}Be this decay channel was first studied theoretically in a cluster model by Baye and Tursonov [6]. The first experimental measurements of this rare decay were reported in Refs. [7–9]. The authors of Ref. [9] obtained a surprisingly large branching ratio for this decay mode, which could only be explained in their analysis if the decay proceeds through a new single-particle resonance in ^{11}B. Their branching ratio was more than two orders of magnitude larger than the cluster model prediction by Baye and Tursunov [6]. As a possible resolution of this discrepancy, Pfützner and Riisager [10] suggested a dark matter decay mode of the valence neutron [11] as the source of the large branching fraction of β-delayed proton emission from ^{11}Be. Thus this rare decay of ^{11}Be would provide a possible avenue to detect a dark matter decay. However, a new experiment by the same collaboration could not reproduce the very large branching ratio b_p and instead provided an upper limit of $b_p < 2.2 \times 10^{-6}$ [12] which is about a factor 4 smaller than the original result.

Recently, Aayad *et al.* [13] remeasured the branching ratio for β-delayed proton emission from ^{11}Be and reported a result similar to that given in Ref. [9]. In particular, they reported a branching ratio of $b_p = (1.3 \pm 0.3) \times 10^{-5}$ and a low-lying resonance with resonance energy $E_R = (196 \pm 20)$ keV with a width of $\Gamma_R = (12 \pm 5)$ keV. Using halo EFT, we have

*elkamhawy@theorie.ikp.physik.tu-darmstadt.de
†hans-werner.hammer@physik.tu-darmstadt.de
‡lplatter@utk.edu

shown that the extracted resonance parameters and decay rate by Ayaad *et al.* are self-consistent [14]. Subsequently, Aayad *et al.* also presented data from a new measurement supporting the existence of a low-lying resonance with $E_R = (171 \pm 20)$ keV and $\Gamma_R = (4.5 \pm 1.1)$ keV in the ^{11}B system [15]. Their resonance energy is consistent with a near-threshold proton resonance in ^{11}B which was observed in the reaction $^{10}\mathrm{Be}(d,n)^{11}\mathrm{B}^* \to {}^{10}\mathrm{Be}+p$ in inverse kinematics [16] and whose resonance energy was estimated to be $E_R = (211 \pm 40)$ keV.

A number of theoretical calculations has recently tried to address the question of the possible existence of a resonance in the proton-^{10}Be system. All approaches that we are aware of indeed found such evidence. A calculation in the shell model embedded in the continuum [17] employed a phenomenological shell model interaction and found evidence for a $1/2^+$ resonance at approximately $E_R \approx 142$ keV, although the large branching ratio into $\beta^- p$ was cast into doubt by a combined study of the $\beta^- p$ and $\beta^- \alpha$ decay channels [18]. Recently, Atkinson *et al.* [19] used the no-core shell model in the continuum to calculate the phase shifts for ^{10}Be-proton scattering in channels of total angular momentum J and parity Π and well-defined total isospin T. Using a chiral effective interaction, the authors adjusted their *ab initio* results to reproduce the ^{11}B resonance position and calculated the branching ratio of the decay into the continuum. Their calculation suggests a definite isospin $T = 1/2$ for the ^{11}B resonance. Finally, a self-consistent Skyrme Hartree-Fock in the continuum also found the near-threshold proton resonance in ^{11}B [20].

One important feature of halo EFT is that observables are parametrized in terms of a few observables. So although the rates for β-delayed proton emission of different halo nuclei can be very different, in first approximation they are governed by the same analytical expressions. Here, we focus on these universal aspects of β-delayed proton emission in halo nuclei. We give results for matrix elements in terms of the few relevant parameters in this problem: the effective range parameters in the initial and final state channels, the mass of the halo nucleus, and the charge of the core nucleus. Due to the large current interest, the main focus is on the application to the β-delayed proton emission from ^{11}Be. However, we also consider the case of ^{19}C as further example.

This paper is organized as follows. In Sec. II, we will set up the halo EFT theoretical framework, which includes the Lagrangian for the system under consideration, the renormalization of the involved coupling constants, and a derivation of the weak matrix elements that are needed. Finally, we end with a summary.

II. HALO EFFECTIVE FIELD THEORY AND WEAK DECAY

In the following, we use natural units with $\hbar = c = 1$. The halo EFT Lagrangian $\mathcal{L}$ for a one-neutron-halo nucleus as well as a low-lying resonance in the core-proton system up to next-to-leading order can be written as $\mathcal{L} = \mathcal{L}_0 + \mathcal{L}_d + \ldots$, where the $\ldots$ indicate higher-order terms in the expansion in $R_{\mathrm{core}}/R_{\mathrm{halo}}$. $\mathcal{L}_0$ is the free Lagrangian of the core, neutron, and proton:

$$\mathcal{L}_0 = c^\dagger\left(i\partial_t + \frac{\nabla^2}{2m_c}\right)c + n^\dagger\left(i\partial_t + \frac{\nabla^2}{2m_n}\right)n + p^\dagger\left(i\partial_t + \frac{\nabla^2}{2m_p}\right)p, \tag{1}$$

where c, n, and p are the core, neutron, and proton fields, respectively. For ^{11}Be, the masses of core, neutron, and proton are given by $m_c = 9327.548$ MeV, $m_n = 939.565$ MeV, and $m_p = 938.272$ MeV. For other $1n$ halos the core mass m_c has to be adjusted accordingly. The leading core-neutron and core-proton interactions are S waves. They are given by

$$\mathcal{L}_d = d_n^\dagger\left[\eta\left(i\partial_t + \frac{\nabla^2}{2M_{nc}}\right) + \Delta\right]d_n + d_p^\dagger\left[\tilde{\eta}\left(i\partial_t + \frac{\nabla^2}{2M_{pc}}\right) + \tilde{\Delta}\right]d_p - g[c^\dagger n^\dagger d_n + \mathrm{H.c.}] - \tilde{g}[c^\dagger p^\dagger d_p + \mathrm{H.c.}], \tag{2}$$

where $M_{nc} = m_n + m_c$ and $M_{pc} = m_p + m_c$. Moreover, d_n and d_p are dimer fields (with suppressed spin indices), which represent the $J^P = 1/2^+$ ground state of the $1n$-halo nucleus and the $J^P = 1/2^+$ low-lying resonance in the core-proton system, respectively. The Lagrangian $\mathcal{L}_d$ contains all terms required up to next-to-leading order (NLO) in the strong interaction sector in the power counting in $R_{\mathrm{core}}/R_{\mathrm{halo}}$. Higher order contributions in the two-body sector will be given by operators with an increasing number of derivatives.

For completeness, the renormalization of the low-energy constants of the S-wave nc system will be briefly summarized (see, e.g., Ref. [21] for details). Due to the nonperturbative nature of the interaction, we need to resum the nc self-energy $\Sigma_{nc}(p_0, \mathbf{p})$ to all orders in order to obtain the halo propagator

$$D_{nc}(p_0, \mathbf{p}) = \left[\Delta + \eta\left(p_0 - \frac{\mathbf{p}^2}{2M_{nc}} + i\epsilon\right) - \Sigma_{nc}(p_0, \mathbf{p})\right]^{-1}. \tag{3}$$

The nc self-energy, evaluated in the power-divergence subtraction scheme, is given by

$$\Sigma_{nc}(p_0, \mathbf{p}) = -\frac{g^2 m_R}{2\pi}\left[i\sqrt{2m_R\left(p_0 - \frac{\mathbf{p}^2}{2M_{nc}}\right)} + \mu\right], \tag{4}$$

where μ is the regularization scale and m_R denotes the reduced mass. The T matrix is then given by $T(E) = g^2 D(E, 0)$ and the low-energy constants appearing in Eq. (2) can be eliminated in favor of the coefficients of the effective range expansion. We then obtain the full two-body T matrix in the center of mass of the neutron-core system

$$T_{nc}(E) = \frac{2\pi}{m_R}\left[\frac{1}{a_0} - r_0 m_R E - \sqrt{-2m_R E - i\epsilon}\right]^{-1}, \tag{5}$$

where a_0 and r_0 are the S-wave core-neutron scattering length and effective range, respectively. This expression holds to NLO in the power counting in $R_{\mathrm{core}}/R_{\mathrm{halo}}$. The corresponding

leading order (LO) result can be obtained by setting $r_0 = 0$.[1] The residue Z of Eq. (5) at the bound state pole is required to calculate physical observables:

$$Z = \frac{2\pi\gamma_0}{m_R^2(1 - r_0\gamma_0)} \tag{6}$$

with $\gamma_0 = (1 - \sqrt{1 - 2r_0/a_0})/r_0 \equiv \sqrt{2m_R S_n}$ the binding momentum of the S-wave halo state, and S_n the one-neutron separation energy of the halo nucleus.

The amplitudes for β decay are obtained through calculation of matrix elements of the electroweak current operator. We include the weak interaction current through the standard product of leptonic and hadronic currents

$$\mathcal{L}_{\text{weak}} = -\frac{G_F}{\sqrt{2}} l_-^\mu ((J_\mu^+)^{1\text{b}} + (J_\mu^+)^{2\text{b}}), \tag{7}$$

where $l_-^\mu = \bar{u}_e \gamma^\mu (1 - \gamma^5) v_{\bar{\nu}}$ and $(J_\mu^+)^{1\text{b}} = (V_\mu^1 - A_\mu^1) + i(V_\mu^2 - A_\mu^2)$ denote the leptonic and hadronic one-body currents, respectively. The hadronic current in halo EFT has one- and two-body contributions. At leading order, the contributions to the hadronic one-body current are $V_0^a = N^\dagger \frac{\tau^a}{2} N$ (Fermi decay), $A_k^a = g_A N^\dagger \frac{\tau^a}{2} \sigma_k N$ (Gamow-Teller decay), where $g_A \simeq 1.27$ denotes the axial-vector coupling constant [22]. Terms with more derivatives will appear at higher orders. When we include resonant core-proton final state interactions, we have to take into account a two-body current with known coupling constants which arises from gauging the time derivative of the dimer fields appearing in Eq. (2). It also decomposes into vector and axial-vector contributions and reads

$$(J_\mu^+)^{2\text{b}} = \begin{cases} -d_p^\dagger d_n & \mu = 0, \\ g_A\, d_p^\dagger \sigma_k d_n & \mu = k = 1, 2, 3. \end{cases} \tag{8}$$

Our EFT approach also predicts also a two-body current with unknown contribution that is denoted as L_{1A}. It usually appears at the same order as the two-body current above. However, in the case with Coulomb interaction, this piece is suppressed by $(R_{\text{core}}/R_{\text{halo}})^{1/2}$ compared to the two-body current in Eq. (8).[2] Therefore, it contributes only at NNLO allowing us to make predictions up to NLO. Note that our power counting including resonant final state interactions implies a suppression of $(R_{\text{core}}/R_{\text{halo}})^{1/2}$ going from order to order instead of $R_{\text{core}}/R_{\text{halo}}$ as in the case without resonant final state interactions.

A. Weak matrix element and decay rate

The decay rate for the decay of the $1n$-halo nucleus into the final particles given by core, proton, electron, and antineutrino expressed via the matrix element $\mathcal{M}$ reads

$$\begin{aligned}\Gamma_p = &\int \frac{d^3p_c}{(2\pi)^3} \int \frac{d^3p_p}{(2\pi)^3} \int \frac{d^3p_e}{(2\pi)^3(2E_e)} \\ &\times \int \frac{d^3p_{\bar{\nu}}}{(2\pi)^3(2E_{\bar{\nu}})} \overline{|\mathcal{M}(\mathbf{p}_c, \mathbf{p}_p, \mathbf{p}_e, \mathbf{p}_{\bar{\nu}})|^2} \\ &\times (2\pi)^4 \delta(S_n - \Delta m + E_c + E_p + E_e + E_{\bar{\nu}}) \\ &\times \delta^3(\mathbf{p}_c + \mathbf{p}_p + \mathbf{p}_e + \mathbf{p}_{\bar{\nu}}),\end{aligned} \tag{9}$$

where $\Delta m = 1.29$ MeV is the mass difference between neutron and proton. Here, $E_e = \sqrt{m_e^2 + \mathbf{p}_e^2}$ is the relativistic on-shell energy of the electron with $m_e = 0.511$ MeV denoting the electron mass, $E_{\bar{\nu}} = |\mathbf{p}_{\bar{\nu}}|$ is the relativistic energy of the antineutrino (assumed to be massless), $E_c = \mathbf{p}_c^2/(2m_c)$ and $E_p = \mathbf{p}_p^2/(2m_p)$ are the nonrelativistic kinetic energies of the core and proton, respectively. Furthermore, $\mathbf{p}_i$ with $i \in \{c, p, e, \bar{\nu}\}$ is the momentum of the corresponding particle. $\overline{|\mathcal{M}|^2}(\mathbf{p}_c, \mathbf{p}_p, \mathbf{p}_e, \mathbf{p}_{\bar{\nu}})$ denotes the squared matrix element summed over final spins and averaged over initial spins. Changing variables, we substitute the coordinates $\mathbf{p}_c$ and $\mathbf{p}_p$ by the relative momentum $\mathbf{p}_{\text{rel}} \equiv \mathbf{p}$ and the total momentum $\mathbf{p}_{\text{tot}}$ of the core-proton system. Moreover, we neglect recoil effects in the energy-conserving δ distribution and then use the momentum-conserving δ distribution to find

$$\begin{aligned}\Gamma_p = &\int \frac{d^3p}{(2\pi)^3} \int \frac{d^3p_e}{(2\pi)^3(2E_e)} \\ &\times \int \frac{d^3p_{\bar{\nu}}}{(2\pi)^3(2E_{\bar{\nu}})} \overline{|\mathcal{M}(\mathbf{p}, -(\mathbf{p}_e + \mathbf{p}_{\bar{\nu}}), \mathbf{p}_e, \mathbf{p}_{\bar{\nu}})|^2} \\ &\times (2\pi)\delta\left(S_n - \Delta m + \frac{\mathbf{p}^2}{2m_R} + E_e + E_{\bar{\nu}}\right).\end{aligned} \tag{10}$$

We define the four-dimensional vector $\tilde{\sigma}_\mu$ consisting of 2×2 matrices for each component,

$$\tilde{\sigma}_\mu = \begin{cases} \mathbb{1}_{2\times 2} & \mu = 0, \\ -g_A\, \sigma_k & \mu = k = 1, 2, 3, \end{cases} \tag{11}$$

and divide the squared matrix element into a purely leptonic and hadronic part. Separating the contribution of the nucleon spin operators, $G_F^2/2\text{Tr}(\tilde{\sigma}_\mu \tilde{\sigma}_\nu^\dagger)$, from the hadronic part we obtain

$$\begin{aligned}\overline{|\mathcal{M}|^2} = &\sum_{\mu,\nu} \sum_{\text{lept.spins}} \left|\mathcal{M}_{\text{lept.}}^{\mu,\nu}(\mathbf{p}_e, \mathbf{p}_{\bar{\nu}})\right|^2 \left(\frac{G_F^2}{2}\text{Tr}(\tilde{\sigma}_\mu \tilde{\sigma}_\nu^\dagger)\right) \\ &\times \frac{1}{2J+1} |\mathcal{A}(\mathbf{p}, -(\mathbf{p}_e + \mathbf{p}_{\bar{\nu}}))|^2,\end{aligned} \tag{12}$$

where $J = 1/2$ denotes the total spin of the S-wave halo nucleus. Further, $|\mathcal{M}_{\text{lept.}}^{\mu,\nu}(\mathbf{p}_e, \mathbf{p}_{\bar{\nu}})|^2$ and $|\mathcal{A}(\mathbf{p}, -(\mathbf{p}_e + \mathbf{p}_{\bar{\nu}}))|^2$ denote the leptonic and hadronic part, respectively. Note that we have already set $\mathbf{p}_{\text{tot}} = -(\mathbf{p}_e + \mathbf{p}_{\bar{\nu}})$. The leptonic part reads

$$\begin{aligned}&\sum_{\text{lept.spins}} \left|\mathcal{M}_{\text{lept.}}^{\mu,\nu}(\mathbf{p}_e, \mathbf{p}_{\bar{\nu}})\right|^2 \\ &= \sum_{\text{lept.spins}} (\bar{u}_e \gamma^\mu (1 - \gamma^5) v_{\bar{\nu}})(\bar{u}_e \gamma^\mu (1 - \gamma^5) v_{\bar{\nu}})^\dagger \qquad (13) \\ &= 8\big(P_e^\mu P_{\bar{\nu}}^\nu + P_e^\nu P_{\bar{\nu}}^\mu - g^{\mu\nu}(P_e \cdot P_{\bar{\nu}})\big), \qquad (14)\end{aligned}$$

[1] For convenience, we do not treat the range r_0 in strict perturbation theory and keep it in the denominator of Eq. (5).

[2] The scaling of $r_0^C \sim 1/k_C$ [23,24] leads to the suppression of the counterterm contribution L_{1A}.

where P_α with $\alpha \in \{e, \bar{\nu}\}$ is the four-momentum of the corresponding particle as indicated by its subscript. Evaluating the trace over spin operators leads to

$$\frac{G_F^2}{2}\mathrm{Tr}(\tilde{\sigma}_\mu \tilde{\sigma}_\nu^\dagger) = \begin{cases} G_F^2 & \mu = \nu = 0, \\ G_F^2\, g_A^2 \delta_{kl} & \mu = k,\ \ \nu = l \ \text{ with } \ k, l \in \{1, 2, 3\}, \\ 0 & \text{otherwise.} \end{cases} \tag{15}$$

From Eq. (15), we conclude that we have a nonvanishing contribution either for $\mu = \nu = 0$ or for $\mu = k$ and $\nu = l$. The first case implies no spin-flip during the decay of the neutron into proton while the latter implies a spin-flip during that transition. The first contribution corresponds to the Fermi and the latter to the Gamow-Teller transition. Note that there is no interference term. Using Eqs. (14) and (15), we find

$$\overline{|\mathcal{M}|^2} = 4G_F^2\big(\sqrt{\mathbf{p}_e^2 + m_e^2}\,|\mathbf{p}_{\bar{\nu}}|\big(1 + 3g_A^2\big) + \mathbf{p}_e \cdot \mathbf{p}_{\bar{\nu}}\big(1 - g_A^2\big)\big) \times |\mathcal{A}(\mathbf{p}, -(\mathbf{p}_e + \mathbf{p}_{\bar{\nu}}))|^2. \tag{16}$$

In order to take into account electromagnetic interactions of the emitted electron with the remaining charged particles, we multiply Eq. (16) with the Sommerfeld factor of the electron given by

$$C^2(\eta_e) = \frac{2\pi\eta_e}{(e^{2\pi\eta_e} - 1)}, \tag{17}$$

where $\eta_e = \alpha Z Z_e E_e/|\mathbf{p}_e|$ with $\alpha = 1/137$ the fine structure constant. We use $Z = Z_p$ in order to ensure that we reproduce the free neutron decay width in the limit of a vanishing one-neutron separation energy of the $1n$-halo nucleus. This means that the electron is only interacting with the outgoing proton. We assume this to be a good approximation since the core is far away from the decaying valence neutron due to the small one-neutron separation energy. The error introduced by this approximation is of higher order (see Ref. [14] for an explicit estimate). Therefore, Eq. (16) becomes

$$\overline{|\mathcal{M}|^2} = 4G_F^2\big(E_e\, E_{\bar{\nu}}\big(1 + 3g_A^2\big) + \mathbf{p}_e \cdot \mathbf{p}_{\bar{\nu}}\big(1 - g_A^2\big)\big) \times |\mathcal{A}(\mathbf{p}, -(\mathbf{p}_e + \mathbf{p}_{\bar{\nu}}))|^2\, C^2(\eta_e). \tag{18}$$

Substituting energies for momenta, integrating out the energy conserving δ function and adjusting the integration momenta accordingly, we then obtain for the decay rate[3]

$$\Gamma_p = \frac{G_F^2}{16\pi^5}\int_0^{\Delta m - S_n - m_e} dE \int_{m_e}^{\Delta m - S_n - E} dE_e \int_{-1}^{1} d\cos\theta \times \int_{-1}^{1} d\cos\theta_{\bar{\nu}}\, m_R\sqrt{2m_R E}$$

[3]A detailed derivation of the rate equation below is given in the Appendix.

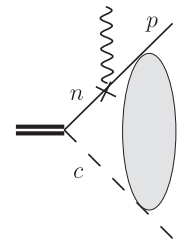

FIG. 1. Feynman diagram for the weak decay of a one-neutron halo nucleus into the corresponding core and a proton with Coulomb final state interactions only. The shaded ellipse denotes the Coulomb ladder diagrams where multiple (including zero) photon exchanges contribute.

$$\times\, E_e\sqrt{E_e^2 - m_e^2}(\Delta m - S_n - E - E_e)^2 \times \big(\big(1 + 3g_A^2\big) + \beta_e \cos\theta_{\bar{\nu}}\big(1 - g_A^2\big)\big) \times |\mathcal{A}(E, E_e, \cos\theta, \cos\theta_{\bar{\nu}})|^2 C^2(\eta_e), \tag{19}$$

where $\boldsymbol{\beta}_e = \mathbf{p}_e/E_e$ and $\boldsymbol{\beta}_{\bar{\nu}} = \mathbf{p}_{\bar{\nu}}/E_{\bar{\nu}}$. The differential decay rate reads

$$\frac{d\Gamma_p}{dE} = \frac{G_F^2}{16\pi^5} m_R\sqrt{2m_R E}\int_{m_e}^{\Delta m - S_n - E} dE_e \times \int_{-1}^{1} d\cos\theta \int_{-1}^{1} d\cos\theta_{\bar{\nu}} \times E_e\sqrt{E_e^2 - m_e^2}(\Delta m - S_n - E - E_e)^2 \times \big(\big(1 + 3g_A^2\big) + \beta_e \cos\theta_{\bar{\nu}}\big(1 - g_A^2\big)\big) \times |\mathcal{A}(E, E_e, \cos\theta, \cos\theta_{\bar{\nu}})|^2 C^2(\eta_e) \tag{20}$$

with

$$0 < E < \Delta m - S_n - m_e. \tag{21}$$

From the partial decay rate we obtain the branching ratio via

$$b_p = \frac{\Gamma_p}{\Gamma}, \tag{22}$$

where $\Gamma = \ln(2)/T_{1/2}$ is the full decay rate and $T_{1/2}$ the half-life of the halo nucleus.

B. Hadronic amplitude without final state interactions

We first consider the hadronic amplitude without final state interactions. It describes the coupling of the electroweak current to the nucleus. For simplicity, we use the momentum variables $\mathbf{p}$, $\mathbf{p}_e$, and $\mathbf{p}_{\bar{\nu}}$ and later apply the constraints from energy and momentum conservation. The corresponding diagram is illustrated in Fig. 1. In halo EFT, the amplitude is derived from the Feynman rules according to the Lagrangians given in Eqs. (1), (2) and (7). The pure hadronic part of Fig. 1 is given by the loop with three propagators, the Coulomb ladder diagrams, the breakup and the wave function renormalization constant of the halo nucleus. After performing the energy integration of the loop, we are left with two propagators. One propagator together with the Coulomb ladder diagrams gives the outgoing Coulomb wave function

$(\tilde{\chi}^-_{\mathbf{p}}(\mathbf{r}))^*$. The other propagator together with the breakup and wave function renormalization constant of the halo nucleus gives the bound state wave function of the $1n$-halo nucleus $\psi(\mathbf{r})$. The pure hadronic amplitude without final state interactions then reads

$$\mathcal{A}(\mathbf{p}, \mathbf{p}_e, \mathbf{p}_{\bar{\nu}}) = -i \int d^3r (\tilde{\chi}^-_{\mathbf{p}}(\mathbf{r}))^* e^{i(1-y)(\mathbf{p}_e+\mathbf{p}_{\bar{\nu}})\cdot\mathbf{r}} \psi(\mathbf{r}), \quad (23)$$

where the exponential function results from the recoil due to the leptons. In general, the Coulomb wave function carries all possible angular momenta l and can be written as

$$(\tilde{\chi}^-_{\mathbf{p}}(\mathbf{r}))^* = \sum_{l=0}^{\infty} \left(\tilde{\chi}^{l-}_{\mathbf{p}}(\mathbf{r})\right)^* = \sum_{l=0}^{\infty} \tilde{\chi}^{l+}_{-\mathbf{p}}(\mathbf{r}) = \sum_{l=0}^{\infty} (-1)^l \, \tilde{\chi}^{l+}_{\mathbf{p}}(\mathbf{r}) \quad (24)$$

with (see Ref. [25])

$$\tilde{\chi}^{l+}_{\mathbf{p}}(\mathbf{r}) = 4\pi i^l e^{i\sigma_l} \frac{F_l(\eta_{|\mathbf{p}|}, |\mathbf{p}|r)}{|\mathbf{p}|r} \sum_{m=-l}^{l} Y^*_{lm}(\mathbf{e}_{\mathbf{p}}) Y_{lm}(\mathbf{e}_{\mathbf{r}}) \quad (25)$$

and

$$F_l(\eta_{|\mathbf{p}|}) = C_l(\eta_{|\mathbf{p}|}) 2^{-l-1} (-i)^{l+1} M_{i\eta_{|\mathbf{p}|}, l+1/2}(2i|\mathbf{p}|r), \quad (26)$$

$$C_l(\eta_{|\mathbf{p}|}) = \frac{2^l e^{-\pi\eta_{|\mathbf{p}|}/2} |\Gamma(l+1+i\eta_{|\mathbf{p}|})|}{\Gamma(2l+2)}, \quad (27)$$

where $M_{k,\mu}(z)$ is the conventionally defined Whittaker function. The Sommerfeld parameter is $\eta_{|\mathbf{p}|} = \alpha Z_p Z_c m_R/|\mathbf{p}| = k_C/|\mathbf{p}|$ while $\sigma_l = \arg(\Gamma(l+1+i\eta_{|\mathbf{p}|}))$ is the Coulomb phase shift. Moreover, the bound state wave function of the neutron-core system is given by

$$\psi(\mathbf{r}) = \sqrt{2\gamma_0} \frac{e^{-\gamma_0 r}}{r} Y_{00}. \quad (28)$$

We use the partial wave expansion of the plane wave

$$e^{i(1-y)(\mathbf{p}_e+\mathbf{p}_{\bar{\nu}})\cdot\mathbf{r}} = 4\pi \sum_{l=0}^{\infty} \sum_{m=-l}^{l} i^l j_l((1-y)|\mathbf{p}_e+\mathbf{p}_{\bar{\nu}}|r) Y_{lm}\left(\mathbf{e}_{\mathbf{p}_e+\mathbf{p}_{\bar{\nu}}}\right) Y^*_{lm}(\mathbf{e}_{\mathbf{r}}), \quad (29)$$

where $j_l(x)$ is a spherical Bessel function. In the low-energy limit, we approximate $j_l(x) \approx (x)^l/(2l+1)!!$. The hadronic amplitude then reads

$$\mathcal{A}(\mathbf{p}, \mathbf{p}_e, \mathbf{p}_{\bar{\nu}}) = -i\sqrt{2\gamma_0}\sqrt{4\pi} \int dr \sum_{l=0}^{\infty} \sum_{m=-l}^{l} re^{-\gamma_0 r} e^{i\sigma_l} \frac{F_l(\eta_{|\mathbf{p}|}, |\mathbf{p}|r)}{|\mathbf{p}|r} \times 4\pi \frac{((1-y)|\mathbf{p}_e+\mathbf{p}_{\bar{\nu}}|r)^l}{(2l+1)!!} Y_{lm}\left(\mathbf{e}_{\mathbf{p}_e+\mathbf{p}_{\bar{\nu}}}\right) Y^*_{lm}(\mathbf{e}_{\mathbf{p}}). \quad (30)$$

The dominant contribution of the hadronic amplitude results from the $l = 0$ transition, meaning no angular momentum between the lepton momentum $(\mathbf{p}_e + \mathbf{p}_{\bar{\nu}})$ and the outgoing relative momentum $\mathbf{p}$. Taking only this contribution into account leads to

$$\mathcal{A}(\mathbf{p}, \mathbf{p}_e, \mathbf{p}_{\bar{\nu}}) = -i\sqrt{8\pi\gamma_0} e^{i\sigma_0} \int dr \, re^{-\gamma_0 r} \frac{F_0(\eta_{|\mathbf{p}|}, |\mathbf{p}|r)}{|\mathbf{p}|r} = -i\sqrt{8\pi\gamma_0} e^{i\sigma_0} C_0(\eta_{|\mathbf{p}|}) \frac{e^{2\eta_{|\mathbf{p}|} \arctan(|\mathbf{p}|/\gamma_0)}}{\gamma_0^2 + |\mathbf{p}|^2}. \quad (31)$$

Higher l transitions correspond to so-called forbidden decays, e.g., the $l = 1$ transition is the first forbidden decay.

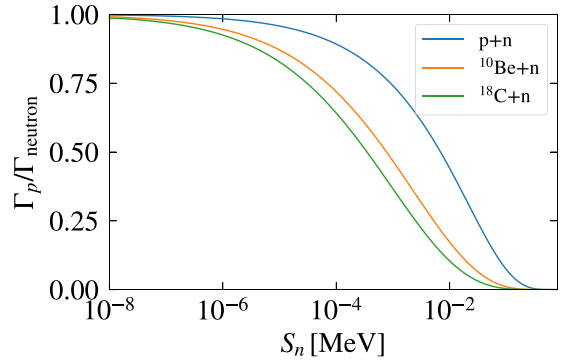

FIG. 2. Partial decay rate without final state interactions at LO relative to the free neutron decay width $\Gamma_p/\Gamma_{\text{neutron}}$ as a function of the one-neutron separation energy S_n for the systems $p+n$, ^{10}Be $+n$, and ^{18}C $+n$.

III. UNIVERSAL RESULTS WITHOUT FINAL STATE INTERACTIONS

The rate for β-delayed proton emission strongly depends on the form of the final state interactions. In the absence of strong final state interactions, this rate is determined predominately by the one-neutron separation energy S_n and the electric charge of the core. We first focus on the latter case.

In Fig. 2, we show the partial decay rate calculated with Eq. (19) in units of the neutron decay rate Γ_{neutron} and in absence of strong final state interactions for systems with different core nuclei as a function of S_n. On the one hand, the results show that the decay rate becomes equal to the free neutron decay rate in the limit of zero one-neutron separation energy for all different systems. In this limit, the halo neutron is not influenced by the core at all and therefore it is expected to give the free neutron decay rate independently of the core properties. On the other hand, the decay rate approaches zero as the one-neutron separation energy increases up to the maximum value given by $S_n^{\max} = m_n - m_p - m_e \approx 782$ keV. This is also expected as the phase space is reduced for increasing S_n. In between these limits, the results show that the decay rate is further reduced for systems with core nuclei of larger sizes with respect to the mass and electric charge. It turns out that the mass dependency is negligible and therefore the reduction of the rate is dominantly given by the increase of the electric charge of the core. This is due to the Coulomb repulsion between the proton and core which is parametrized through the Sommerfeld factor $C_0(\eta_{|\mathbf{p}|})$. It leads to a reduction of the differential decay rate $d\Gamma_p/dE$ especially for low relative energies E of the charged particles. Hence, the behaviour

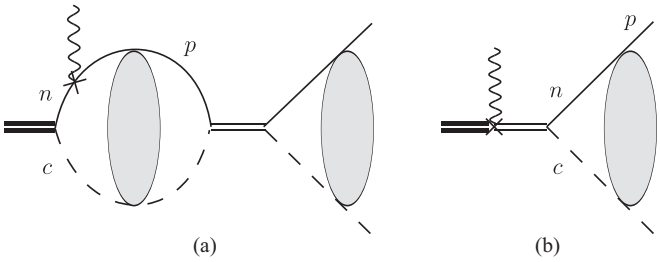

FIG. 3. Feynman diagrams for the weak decay of a one-neutron halo nucleus into the corresponding core and a proton with strong final state interactions. The thin double line in the middle denotes the dressed $^{10}\mathrm{Be}-p$ propagator. The shaded ellipse denotes the Coulomb ladder diagrams where multiple (including zero) photon exchanges contribute.

for different systems universally depends on the charge of the core. Next we focus on the case with final state interactions.

IV. RESULTS WITH FINAL STATE INTERACTIONS FOR BERYLLIUM-11

As laid out above, halo EFT can not predict by itself whether the resonance exists but instead provides a consistency check between different observables in the resonance region. In Ref. [14], we performed an analysis of the impact of a resonance on the branching ratio. In this analysis, it was assumed that the resonance has no definite isospin. We briefly summarize our results for this scenario. Using the central value and errors of the resonance energy from the recent publication [15], the branching ratio and the resonance width were determined to be $b_p = (1.2^{+1.1}_{-0.6}(\mathrm{exp.})^{+0.9}_{-0.2}(\mathrm{theo.})) \times 10^{-5}$ and $\Gamma_R = (5.0^{+3.0}_{-2.1}(\mathrm{exp.})^{+3.1}_{-1.1}(\mathrm{theo.}))\,\mathrm{keV}$. Based on the value and errors for the resonance energy published previously [13], we obtain $b_p = (4.9^{+5.6}_{-2.9}(\mathrm{exp.})^{+4.0}_{-0.8}(\mathrm{theo.})) \times 10^{-6}$ and $\Gamma_R = (9.0^{+4.8}_{-3.3}(\mathrm{exp.})^{+5.3}_{-2.2}(\mathrm{theo.}))\,\mathrm{keV}$. These results are consistent within the combined theoretical and experimental uncertainties. Next we analyze the scenario of a $^{11}\mathrm{B}$ resonance with definite isospin of $T = 1/2$. The additional diagrams due to the resonance are depicted in Fig. 3. Starting with the Lagrangian given in Eqs. (1) and (2), we project the $^{10}\mathrm{Be}-p$ interaction on $T = 1/2$. Therefore, it is ensured that only the $T = 1/2$ channel is resonant. As a consequence, the isospin changes during the decay. This implies that the transition is a pure Gamow-Teller transition. Moreover, this projection impacts the β-strength sum rule that counts the number of weak charges that can decay in the initial state. The Gamow-Teller strength B_{GT} is related to the comparative half-lives or ft value of the decay. The ft value itself is given by

$$ft = \frac{B}{g_A^2 B_{\mathrm{GT}}}, \tag{32}$$

where $B = 2\pi^3 \ln 2/(m_e^5 G_F^2)$ is the β-decay constant. Here, we use the value $B = 6144.2$ s [26,27]. The inverse ft value can be obtained from the transition matrix element $\mathcal{M}$ of $^{11}\mathrm{Be}$ into $^{10}\mathrm{Be}+p$ via the relation

$$\frac{1}{ft} = \frac{1}{B}\overline{|\mathcal{M}|^2} = \frac{1}{B}\frac{(1+3g_A^2)}{2\pi^2}\int dE\, m_R\sqrt{2m_R E}\;\overline{|\mathcal{A}(\mathbf{p})|^2}. \tag{33}$$

For a transition into the continuum, the differential Gamow-Teller β strength can then be calculated from

$$\frac{dB_{\mathrm{GT}}}{dE} = \frac{(1+3g_A^2)}{g_A^2}\frac{1}{2\pi^2}\, m_R\sqrt{2m_R E}\;\overline{|\mathcal{A}(\mathbf{p})|^2}. \tag{34}$$

Integration over the whole continuum gives the β-strength sum rule that we require to be fulfilled at each order within our EFT power counting. We note that a resonance with no definite isospin in the halo picture leads to the sum rule $B_{\mathrm{F}}^{\mathrm{max}} = 1$ and $B_{\mathrm{GT}}^{\mathrm{max}} = 3$ (see Ref. [14]) accounting for the halo neutron that can decay in the initial channel. However, after projecting on a resonance with $T = 1/2$, we do not fully count the weak charge that can decay in the initial channel and therefore expect to have $B_{\mathrm{GT}}^{\mathrm{max}} < 3$ for the β-strength sum rule. At LO where the full nonperturbative solution for a zero-range interaction is used in the incoming as well as outgoing channels, we indeed find the sum rule satisfying $B_{\mathrm{GT}}^{\mathrm{max}} < 3$. When integrating over the available Q window, we therefore expect $B_{\mathrm{GT}} < B_{\mathrm{GT}}^{\mathrm{max}} < 3$. At NLO range corrections enter. However, the sum rule $B_{\mathrm{GT}}^{\mathrm{max}}$ derived at LO puts strong constraints on the ranges in the incoming and outgoing channels. As a consequence, only certain combinations are allowed. In Fig. 4, we present the resonance parameter combinations that satisfy the β-strength sum rule at LO and at NLO. The dash-dotted line gives the LO result where all ranges are zero. At NLO, we use $r_0 = 2.7$ fm for the incoming channel, which was determined from the measured $B(E1)$ strength for Coulomb dissociation of $^{11}\mathrm{Be}$ [21]. Using the one-neutron separation energy and the effective range of $^{11}\mathrm{Be}$, the GT sum rule can be fulfilled only for a Coulomb-modified effective range in the outgoing channel of $r_0^C = 1.8$ fm. The sum rule is then satisfied to very

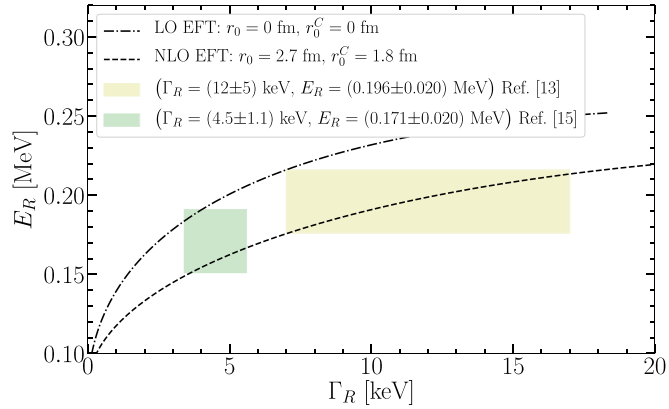

FIG. 4. Possible resonance parameter combinations obeying the sum rule obtained in the halo EFT approach with isospin projection. The dash-dotted line shows the combinations for $r_0 = 0$ fm at LO corresponding to $r_0^C = 0$ fm while the dashed line shows the combinations for $r_0 = 2.7$ fm at NLO corresponding to $r_0^C = 1.8$ fm. The green and yellow band show the resonance parameters given in Refs. [13,15].

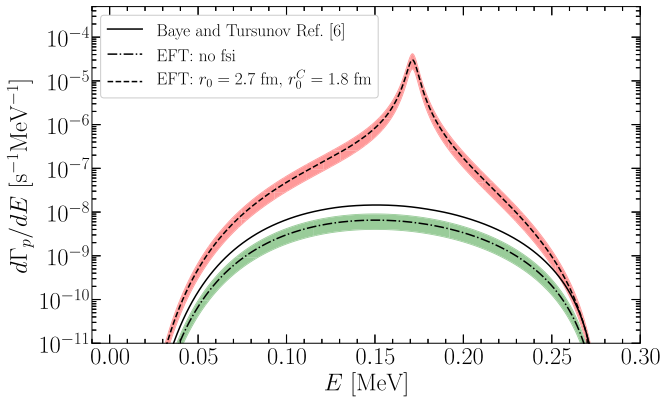

FIG. 5. Differential decay rate $d\Gamma_p/dE$ for β-delayed proton emission from ^{11}Be as a function of the final-state particle energy E. The dash-dotted line shows our EFT result without resonant final state interactions while the solid line gives the result obtained by Baye and Tursunov [6]. The dashed line shows the EFT result including a resonance at $E_R = 0.171$ MeV in the outgoing channel at NLO. The colored bands give the EFT uncertainty.

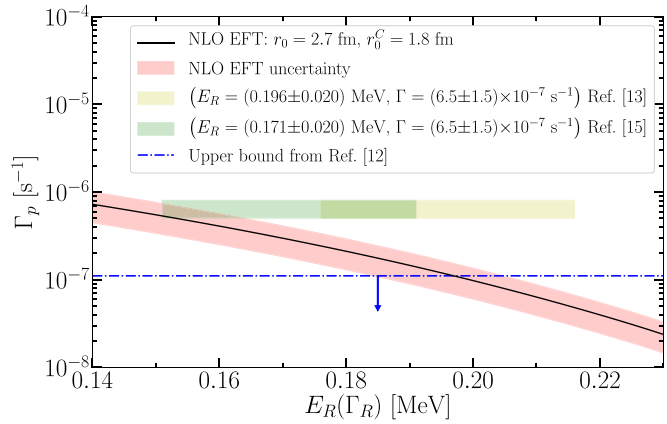

FIG. 6. Partial decay rate as a function of the resonance energy at NLO. Explanation of curves and bands is given in inset.

good approximation for a wide range of Coulomb-modified scattering lengths in the outgoing channel. In particular, both sets of resonance parameters from Refs. [13,15] are consistent with the constraints on E_R and Γ_R provided by our halo EFT calculation, although there is some tension between the two measurements themselves.

The effect of the resonance on the decay rate can be visualized by looking at the differential decay rate $d\Gamma_p/dE$ as shown in Fig. 5. The dash-dotted line shows the EFT result in the absence of any final state interactions. The dashed line shows the differential decay rate with a resonance at $E_R = 0.171$ MeV [15] and effective ranges in initial and final state fixed as discussed above. The rapid fall off of the differential decay rate at energies below $\sim$0.08 MeV and above $\sim$0.21 MeV, and the noticeable enhancement of the decay rate requires a resonance that also approximately lies in the same window. Using the value and its errors for the resonance energy published in Ref. [15], $E_R = (171 \pm 20)$ keV, we find

$$b_p = \left(5.7^{+5.0}_{-2.9}(\text{exp.})^{+4.1}_{-1.1}(\text{theo.})\right) \times 10^{-6}, \quad \log(ft) = 3.37,$$
$$\Gamma_R = \left(6.2^{+3.8}_{-2.6}(\text{exp.})^{+3.9}_{-1.4}(\text{theo.})\right) \text{keV}, \qquad B_{\text{GT}} = 1.63.$$

We have also analyzed the impact of a resonance using $E_R = (196 \pm 20)$ keV [13] leading to a similar plot as in Fig. 5 with a peak position at the corresponding resonance energy. Using the value and its errors for the resonance energy published in Ref. [13], we find

$$b_p = \left(2.3^{+2.5}_{-1.3}(\text{exp.})^{+1.8}_{-0.4}(\text{theo.})\right) \times 10^{-6}, \quad \log(ft) = 3.38,$$
$$\Gamma_R = \left(11.3^{+6.9}_{-4.2}(\text{exp.})^{+7.0}_{-2.7}(\text{theo.})\right) \text{keV}, \qquad B_{\text{GT}} = 1.59.$$

Again both sets of values are consistent within their uncertainties.

In Fig. 6, we show the partial decay rate for beta-delayed proton emission from ^{11}Be as a function of the resonance energy. The solid line gives our NLO result with the effective range parameters set as described above. The yellow and green squares give the experimental result given in Refs. [13,15], respectively. The partial decay rate decreases as the resonance energy increases and moves out of the energy range described above. The overlap of the green square and our EFT predictions shows that our results are consistent with the results for the decay rate published by Ayyad *et al.* [13] when using the new resonance parameters determined in [15]. However, there is some tension when the resonance parameters from [13] are used. For resonance energies larger than $\sim$200 keV the upper bound on the partial width from Riisager *et al.* [12] is satisfied. When using the resonance energies determined in Ref. [16] given by $E_R = (211 \pm 40)$ keV leads to decay rates that are mostly in agreement with that upper bound.

V. RESULTS FOR CARBON-19

As another example, we consider beta-delayed proton emission from the 1n-halo nucleus ^{19}C. In contrast to the case of ^{11}Be, there is no clear separation of scales between the half-lives of ^{19}C which has $T_{1/2} = 46.3$ ms and of the ^{18}C core which has $T_{1/2} = 92 \pm 2$ ms. However, the process of β-delayed proton emission can still be observed by measuring the ^{18}C core and the proton in the final state. Even if the ^{18}C core of the 1n-halo nucleus ^{19}C β decays into the ground state of ^{18}N, it cannot feed into the observed decay channel due to energy conservation since $m_{^{18}C} + m_p - (m_{^{18}N} + m_n) \approx 10.5$ MeV. We assume the contributions from decay channels via excited states of ^{18}N* to be insignificant.

In Fig. 7, we show the differential decay rate as a function of the energy E without resonant final state interactions. Our results for ^{19}C agree qualitatively with those presented by Baye and Tursunov [6]. The corresponding branching ratio is

$$b_p = (4.1 \pm 2.5) \times 10^{-14}. \tag{35}$$

For comparison, the branching ratio for β-delayed proton emission from ^{11}Be without resonant final state interactions is given by 1.3×10^{-8}. Therefore, the branching ratio for ^{19}C is almost six orders smaller than for ^{11}Be without final state interactions. This smaller branching ratio results from the larger

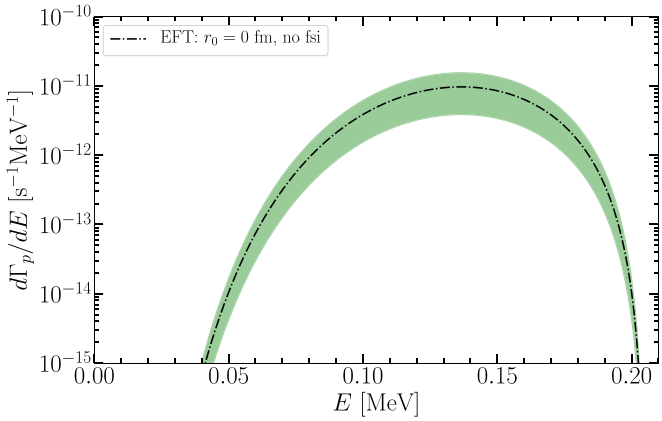

FIG. 7. Differential decay rate $d\Gamma_p/dE$ for β-delayed proton emission from ^{19}C as a function of the final-state particle energy E. The dash-dotted line shows our EFT result without resonant final state interactions. The green band gives the EFT uncertainty.

separation energy of ^{19}C ($S_n = 0.577$ MeV), the larger charge number (see discussion in Sec. III), and the overall larger total decay rate of ^{19}C. The branching ratio could be in principle enlarged by a ^{19}N* resonance but we do not consider this effect since no resonances are known in the decay window. Our result for the branching ratio is approximately by a factor of three smaller than that given by Baye and Tursunov [6] who give a value of 1.8×10^{-13} from a cluster model that includes some final state interactions.

VI. SUMMARY

In this paper, we considered β-delayed proton emission in one-neutron halo nuclei in the framework of halo EFT. We discussed the general features of the relevant matrix elements in systems that do not have strong final state interactions and in systems that display strong final state interactions due to a low-lying resonance in the proton-core channel. In the scenario of no strong final state interactions, we found that the decay rate predominantly depends on the one-neutron separation energy and the electric charge of the core. Including strong final state interactions via a resonance in the proton-core channel can have a significant impact on the decay rate depending on the resonance position. If it lies within the *energy window* defined by the plateau of the differential decay rate without strong final state interactions, it leads to a significant enhancement of the decay rate and hence the branching ratio. We found that for heavier halo nuclei, a significantly enhanced branching ratio for a given one-neutron separation energy becomes more unlikely. The bigger charge of the core nucleus leads to an increased Coulomb repulsion between core and proton at low relative energies E. Thus, the differential decay rate for low E is reduced and therefore the *energy window* for the required resonance energies in order to significantly enhance the branching ratio becomes smaller. The calculations with strong final state interactions were done with and without isospin projection on states of definite isospin.

We have also presented additional details of the calculation for the decay of ^{11}Be previously published in Ref. [14]. Furthermore, we reanalyzed our results in the context of recently published data [15]. We found that the measured resonance parameters of the low-lying resonance in the ^{11}B system is consistent with the measured branching ratio for the β decay of ^{11}Be into the continuum but that theory and experiment do not overlap perfectly. We also stress again that our results do not imply the existence of the low-lying resonance but that a resonance is required for an enhanced branching ratio of β-delayed proton emission.

Halo EFT seems generally well suited for the analysis of this framework: Observables can be calculated in terms of a small number of parameters that are determined from experiment. The number of parameters used in such a calculation is also inherently tied to the uncertainty for the observable of interest. In contradistinction to cluster models, two-body currents appear naturally in this framework. For example, a two-body axial current will appear one order higher than what was considered in this work [28]. A higher order calculation in halo EFT is therefore unpractical since the unknown parameter would have to be determined from the β decay itself. However, this limitation is shared with other approaches such as calculations of this process in chiral EFT with electroweak currents. In this framework such a two-body current also appears at next-to-next-to-leading order in the chiral expansion [29], the same order that the chiral three-nucleon force enters which is required for the accurate description of nuclear structure observables [30]. Furthermore, we note that our approach implies that any cluster model with the same degrees of freedom but without additional microscopic physics will have at best the uncertainty as our results.

There are several important questions that need to be addressed in the future. For example, it needs to be analyzed whether a meaningful calculation can be carried out for P-wave halo nuclei. In such systems, the counting of interaction operators and current operators changes nontrivially. It is therefore not clear whether halo EFT or any cluster approach can predict the lifetime accurately, however, it provides nonetheless a complementary approach to study the decay itself. It would also be interesting to apply halo EFT to weak decays of two-neutron halo systems. Such a calculation has been done using a cluster model [31]. A halo EFT calculation could shine light on the uncertainties of this calculation.

ACKNOWLEDGMENTS

This work has been supported by the National Science Foundation under Grants No. PHY-1555030 and No. PHY-2111426, by the Office of Nuclear Physics, U.S. Department of Energy under Contract No. DE-AC05-00OR22725, by the Deutsche Forschungsgemeinschaft (DFG, German Research Foundation) – Projektnummer 279384907 – CRC 1245, and by the German Federal Ministry of Education and Research (BMBF) (Grant No. 05P21RDFNB).

APPENDIX: DERIVATION OF THE DECAY RATE

We choose the z axis of the coordinate system in which we perform the $\mathbf{p}_{\bar{\nu}}$ integration to be parallel to the momentum $\mathbf{p}_e$. Therefore, the scalar product $\boldsymbol{\beta}_e \cdot \boldsymbol{\beta}_{\bar{\nu}} = |\boldsymbol{\beta}_e||\boldsymbol{\beta}_{\bar{\nu}}| \cos\theta_{\bar{\nu}} \equiv \beta_e \beta_{\bar{\nu}} \cos\theta_{\bar{\nu}} = \beta_e \cos\theta_{\bar{\nu}}$. Moreover, we choose the z axis of the coordinate system in which we perform the $\mathbf{p}$ integration to be parallel to the momentum $(\mathbf{p}_e + \mathbf{p}_{\bar{\nu}})$. We denote the angle between $\mathbf{p}$ and $(\mathbf{p}_e + \mathbf{p}_{\bar{\nu}})$ as θ. As a consequence, the hadronic amplitude depends on $|\mathbf{p}|$ and $|\mathbf{p}_e + \mathbf{p}_{\bar{\nu}}|$ and $\cos\theta$. Since

$$|\mathbf{p}_e + \mathbf{p}_{\bar{\nu}}| = \sqrt{\mathbf{p}_e^2 + \mathbf{p}_{\bar{\nu}}^2 + 2|\mathbf{p}_e||\mathbf{p}_{\bar{\nu}}| \cos\theta_{\bar{\nu}}}, \tag{A1}$$

the hadronic amplitude will ultimately depend on $|\mathbf{p}|$, $|\mathbf{p}_e|$, $|\mathbf{p}_{\bar{\nu}}|$, $\cos\theta$, and $\cos\theta_{\bar{\nu}}$ and therefore we replace

$$|\mathcal{A}(\mathbf{p}, -(\mathbf{p}_e + \mathbf{p}_{\bar{\nu}}))|^2 \;\rightarrow\; |\mathcal{A}(|\mathbf{p}|, |\mathbf{p}_e|, |\mathbf{p}_{\bar{\nu}}|, \cos\theta, \cos\theta_{\bar{\nu}})|^2 \tag{A2}$$

and find

$$\begin{aligned}\Gamma_p = \frac{G_F^2}{(2\pi)^8} \int d^3p \int d^3p_e \int d^3p_{\bar{\nu}} \delta\left(S_n - \Delta m + \frac{\mathbf{p}^2}{2m_R} + \sqrt{\mathbf{p}_e^2 + m_e^2} + |\mathbf{p}_{\bar{\nu}}|\right) \\ \times \left(\left(1 + 3g_A^2\right) + \beta_e \cos\theta_{\bar{\nu}}\left(1 - g_A^2\right)\right) |\mathcal{A}(|\mathbf{p}|, |\mathbf{p}_e|, |\mathbf{p}_{\bar{\nu}}|, \cos\theta, \cos\theta_{\bar{\nu}})|^2 C^2(\eta_e).\end{aligned} \tag{A3}$$

Now we perform the trivial angle integrations, meaning

$$\int d^3p \rightarrow 2\pi \int_0^\infty dp\, \mathbf{p}^2 \int_{-1}^1 d\cos\theta, \tag{A4}$$

$$\int d^3p_e \rightarrow 4\pi \int_0^\infty dp_e\, \mathbf{p}_e^2, \tag{A5}$$

$$\int d^3p_{\bar{\nu}} \rightarrow 2\pi \int_0^\infty dp_{\bar{\nu}}\, \mathbf{p}_{\bar{\nu}}^2 \int_{-1}^1 d\cos\theta_{\bar{\nu}}, \tag{A6}$$

and get

$$\begin{aligned}\Gamma_p = \frac{G_F^2}{16\pi^5} \int_0^\infty dp \mathbf{p}^2 \int_{-1}^1 d\cos\theta \int_0^\infty dp_e \mathbf{p}_e^2 \int_0^\infty dp_{\bar{\nu}} \mathbf{p}_{\bar{\nu}}^2 \int_{-1}^1 d\cos\theta_{\bar{\nu}} \\ \times\, \delta\left(S_n - \Delta m + \frac{\mathbf{p}^2}{2m_R} + \sqrt{\mathbf{p}_e^2 + m_e^2} + |\mathbf{p}_{\bar{\nu}}|\right)\left(\left(1 + 3g_A^2\right) + \beta_e \cos\theta_{\bar{\nu}}\left(1 - g_A^2\right)\right) \\ \times\, |\mathcal{A}(|\mathbf{p}|, |\mathbf{p}_e|, |\mathbf{p}_{\bar{\nu}}|, \cos\theta, \cos\theta_{\bar{\nu}})|^2 C^2(\eta_e).\end{aligned} \tag{A7}$$

Using the energy-conserving δ distribution

$$|\mathbf{p}_{\bar{\nu}}| \;\rightarrow\; \left(\Delta m - S_n - \frac{\mathbf{p}^2}{2m_R} - \sqrt{\mathbf{p}_e^2 + m_e^2}\right) \equiv |\overline{\mathbf{p}}_{\bar{\nu}}|, \tag{A8}$$

we perform the $p_{\bar{\nu}}$ integration to find

$$\begin{aligned}\Gamma_p = \frac{G_F^2}{16\pi^5} \int_0^\infty dp \int_0^\infty dp_e \int_{-1}^1 d\cos\theta \int_{-1}^1 d\cos\theta_{\bar{\nu}} \mathbf{p}^2 \mathbf{p}_e^2 |\overline{\mathbf{p}}_{\bar{\nu}}|^2 \Theta(|\overline{\mathbf{p}}_{\bar{\nu}}|) \\ \times \left(\left(1 + 3g_A^2\right) + \beta_e \cos\theta_{\bar{\nu}}\left(1 - g_A^2\right)\right) |\mathcal{A}(|\mathbf{p}|, |\mathbf{p}_e|, |\overline{\mathbf{p}}_{\bar{\nu}}|, \cos\theta, \cos\theta_{\bar{\nu}})|^2 C^2(\eta_e),\end{aligned} \tag{A9}$$

where Θ is the Heaviside step function. Since $|\overline{\mathbf{p}}_{\bar{\nu}}|$ depends on $\mathbf{p}$ and $\mathbf{p}_e$, we replace

$$|\mathcal{A}(|\mathbf{p}|, |\mathbf{p}_e|, |\overline{\mathbf{p}}_{\bar{\nu}}|, \cos\theta, \cos\theta_{\bar{\nu}})|^2 \;\rightarrow\; |\mathcal{A}(|\mathbf{p}|, |\mathbf{p}_e|, \cos\theta, \cos\theta_{\bar{\nu}})|^2 \tag{A10}$$

and get

$$\begin{aligned}\Gamma_p = \frac{G_F^2}{16\pi^5} \int_0^\infty dp \int_0^\infty dp_e \int_{-1}^1 d\cos\theta \int_{-1}^1 d\cos\theta_{\bar{\nu}} \mathbf{p}^2 \mathbf{p}_e^2 |\overline{\mathbf{p}}_{\bar{\nu}}|^2 \Theta(|\overline{\mathbf{p}}_{\bar{\nu}}|) \\ \times \left(\left(1 + 3g_A^2\right) + \beta_e \cos\theta_{\bar{\nu}}\left(1 - g_A^2\right)\right) |\mathcal{A}(|\mathbf{p}|, |\mathbf{p}_e|, \cos\theta, \cos\theta_{\bar{\nu}})|^2 C^2(\eta_e).\end{aligned} \tag{A11}$$

Substituting

$$\int_0^\infty dp\, \mathbf{p}^2 = \int_0^\infty dE\; m_R \sqrt{2m_R E}, \tag{A12}$$

$$\int_0^\infty dp_e\, \mathbf{p}_e^2 = \int_{m_e}^\infty dE_e\, E_e\sqrt{E_e^2 - m_e^2}, \tag{A13}$$

where $E = \mathbf{p}^2/(2m_R)$ is the relative energy of the core-proton system and replacing

$$|\mathcal{A}(|\mathbf{p}|, |\mathbf{p}_e|, \cos\theta, \cos\theta_{\bar\nu})|^2 \;\to\; |\mathcal{A}(E, E_e, \cos\theta, \cos\theta_{\bar\nu})|^2 \tag{A14}$$

we find

$$\Gamma_p = \frac{G_F^2}{16\pi^5}\int_0^\infty dE \int_{m_e}^\infty dE_e \int_{-1}^1 d\cos\theta \int_{-1}^1 d\cos\theta_{\bar\nu} m_R\sqrt{2m_R E}E_e\sqrt{E_e^2 - m_e^2}$$
$$\times\; (\Delta m - S_n - E - E_e)^2\Theta(\Delta m - S_n - E - E_e)\big(\big(1 + 3g_A^2\big) + \beta_e\cos\theta_{\bar\nu}\big(1 - g_A^2\big)\big)|\mathcal{A}(E, E_e, \cos\theta, \cos\theta_{\bar\nu})|^2 C^2(\eta_e). \tag{A15}$$

Finally, we apply the Θ function by modifying the integration areas

$$\Gamma_p = \frac{G_F^2}{16\pi^5}\int_0^{\Delta m - S_n - m_e} dE \int_{m_e}^{\Delta m - S_n - E} dE_e \int_{-1}^1 d\cos\theta \int_{-1}^1 d\cos\theta_{\bar\nu} m_R\sqrt{2m_R E}$$
$$\times\; E_e\sqrt{E_e^2 - m_e^2}(\Delta m - S_n - E - E_e)^2\big(\big(1 + 3g_A^2\big) + \beta_e\cos\theta_{\bar\nu}\big(1 - g_A^2\big)\big)|\mathcal{A}(E, E_e, \cos\theta, \cos\theta_{\bar\nu})|^2 C^2(\eta_e). \tag{A16}$$

If we do not neglect recoil effects, then there is an additional term $(\mathbf{p}_e + \mathbf{p}_{\bar\nu}^2)/(2M_{pc})$ in the energy-conserving δ distribution of Eq. (A7). Performing a similar calculation as before, we find for the decay rate

$$\Gamma_p = \frac{G_F^2 M_{pc}}{16\pi^5}\int_0^{\Delta m - S_n - m_e} dE\; m_R\sqrt{2m_R E}\int_{-1}^1 d\cos\theta \int_{m_e}^{E_e^{\rm upper}} dE_e\, E_e \int_{E_{\bar\nu}^{\rm lower}}^{E_{\bar\nu}^{\rm upper}} dE_{\bar\nu}\, E_{\bar\nu}$$
$$\times\; \big(\big(1 + 3g_A^2\big) + \beta_e\overline{\cos\theta_{\bar\nu}}\big(1 - g_A^2\big)\big)\,|\mathcal{A}(E, \cos\theta, E_e, E_{\bar\nu}, \overline{\cos\theta_{\bar\nu}})|^2\, C^2(\eta_e) \tag{A17}$$

with

$$E_{\bar\nu}^{\rm lower} = \sqrt{(\Delta m - S_n - E - E_e)2M_{pc} - \big(E_e^2 - m_e^2\big) + \big(M_{pc} + \sqrt{E_e^2 - m_e^2}\big)^2} - \big(M_{pc} + \sqrt{E_e^2 - m_e^2}\big), \tag{A18}$$

$$E_{\bar\nu}^{\rm upper} = \sqrt{(\Delta m - S_n - E - E_e)2M_{pc} - \big(E_e^2 - m_e^2\big) + \big(M_{pc} - \sqrt{E_e^2 - m_e^2}\big)^2} - \big(M_{pc} - \sqrt{E_e^2 - m_e^2}\big), \tag{A19}$$

and

$$E_e^{\rm lower} = m_e, \tag{A20}$$

$$E_e^{\rm upper} = \sqrt{(\Delta m - S_n - E)2M_{pc} + m_e^2 + M_{pc}^2} - M_{pc}. \tag{A21}$$

[1] C. A. Bertulani, H. W. Hammer, and U. Van Kolck, Nucl. Phys. A **712**, 37 (2002).
[2] P. F. Bedaque, H. W. Hammer, and U. van Kolck, Phys. Lett. B **569**, 159 (2003).
[3] H. W. Hammer, C. Ji, and D. R. Phillips, J. Phys. G **44**, 103002 (2017).
[4] H. W. Hammer, S. König, and U. van Kolck, Rev. Mod. Phys. **92**, 025004 (2020).
[5] H.-W. Hammer, Theory of Halo nuclei, in *Handbook of Nuclear Physics*, edited by I. Tanihata, H. Toki, and T. Kajino (Springer, Singapore, 2022), pp. 1–30.
[6] D. Baye and E. M. Tursunov, Phys. Lett. B **696**, 464 (2011).
[7] M. J. G. Borge, L. M. Fraile, H. O. U. Fynbo, B. Jonson, O. S. Kirsebom, T. Nilsson, G. Nyman, G. Possnert, K. Riisager, and O. Tengblad, J. Phys. G **40**, 035109 (2013).
[8] K. Riisager (IS541 Collaboration), EPJ Web Conf. **66**, 02090 (2014).
[9] K. Riisager *et al.*, Phys. Lett. B **732**, 305 (2014).
[10] M. Pfützner and K. Riisager, Phys. Rev. C **97**, 042501(R) (2018).
[11] B. Fornal and B. Grinstein, Phys. Rev. Lett. **120**, 191801 (2018); **124**, 219901(E) (2020).
[12] K. Riisager *et al.*, Eur. Phys. J. A **56**, 100 (2020).
[13] Y. Ayyad *et al.*, Phys. Rev. Lett. **123**, 082501 (2019); **124**, 129902(E) (2020).
[14] W. Elkamhawy, Z. Yang, H.-W. Hammer, and L. Platter, Phys. Lett. B **821**, 136610 (2021).
[15] Y. Ayyad *et al.*, Phys. Rev. Lett. **129**, 012501 (2022).
[16] E. Lopez-Saavedra *et al.*, Phys. Rev. Lett. **129**, 012502 (2022).
[17] J. Okołowicz, M. Płoszajczak, and W. Nazarewicz, Phys. Rev. Lett. **124**, 042502 (2020).

[18] J. Okołowicz, M. Płoszajczak, and W. Nazarewicz, J. Phys. G **49**, 10LT01 (2022).
[19] M. C. Atkinson, P. Navrátil, G. Hupin, K. Kravvaris, and S. Quaglioni, Phys. Rev. C **105**, 054316 (2022).
[20] N. Le Anh, B. M. Loc, N. Auerbach, and V. Zelevinsky, Phys. Rev. C **106**, L051302 (2022).
[21] H. W. Hammer and D. R. Phillips, Nucl. Phys. A **865**, 17 (2011).
[22] C. C. Chang *et al.*, Nature (London) **558**, 91 (2018).
[23] E. Ryberg, C. Forssén, H. W. Hammer, and L. Platter, Ann. Phys. **367**, 13 (2016).
[24] C. H. Schmickler, H. W. Hammer, and A. G. Volosniev, Phys. Lett. B **798**, 135016 (2019).
[25] R. Higa, G. Rupak, and A. Vaghani, Eur. Phys. J. A **54**, 89 (2018).
[26] M. Pfützner, M. Karny, L. V. Grigorenko, and K. Riisager, Rev. Mod. Phys. **84**, 567 (2012).
[27] J. C. Hardy and I. S. Towner, Phys. Rev. C **71**, 055501 (2005).
[28] X. Kong and F. Ravndal, Phys. Rev. C **64**, 044002 (2001).
[29] T.-S. Park, H. Jung, and D.-P. Min, Phys. Lett. B **409**, 26 (1997).
[30] H.-W. Hammer, A. Nogga, and A. Schwenk, Rev. Mod. Phys. **85**, 197 (2013).
[31] E. M. Tursunov, D. Baye, and P. Descouvemont, Phys. Rev. C **97**, 014302 (2018).